Title

Excitation Intensity Dependence of Photoluminescence Blinking in CsPbBr3 Perovskite Nanocrystals

Journal

Journal of Physical Chemistry C, 122(22)

ISSN

1932-7447

Authors

Gibson, NA
Koscher, BA
Alivisatos, AP
et al.

Publication Date

2018-06-07

DOI

10.1021/acs.jpcc.8b03206

Excitation Intensity Dependence of Photoluminescence Blinking in $CsPbBr_3$ Perovskite Nanocrystals

Natalie A. Gibson,[†,||,⊥] *Brent A. Koscher,*[†,§,⊥,#] *A. Paul Alivisatos,*[†,§,⊥,#] *Stephen R. Leone*[*,†,‡,||,⊥]

[†]Department of Chemistry, [‡]Department of Physics, and [§]Department of Materials Science and Engineering, University of California, Berkeley, Berkeley, California 94720, United States

[||]Chemical Sciences Division and [⊥]Materials Sciences Division, Lawrence National Berkeley Laboratory, Berkeley, California 94720, United States

[#]Kavli Energy NanoScience Institute, Berkeley, California 94720, United States

ABSTRACT

Perovskite semiconductors have emerged as a promising class of materials for optoelectronic applications. Their favorable device performances can be partly justified by the defect tolerance that originates from their electronic structure. The effect of this inherent defect tolerance, namely the absence of deep trap states, on the photoluminescence (PL) of perovskite nanocrystals (NCs) is currently not well understood. The PL emission of NCs fluctuates in time according to power law kinetics (PL intermittency, or blinking), a phenomenon that has been explored over the past two decades in a vast array of nanocrystal (NC) materials. The kinetics of the blinking process in perovskite NCs have not been widely explored. Here, PL trajectories of individual orthorhombic cesium lead bromide ($CsPbBr_3$) perovskite NCs are measured using a range of excitation intensities. The power law kinetics of the bright NC state are observed to truncate exponentially at long durations, with a truncation time that decreases with increasing intensity before saturating at a single exciton intensity. The results indicate that a diffusion-controlled electron transfer (DCET) mechanism is the most likely charge trapping process, while Auger autoionization plays a lesser role. Further experimentation and theoretical work are needed to gain a comprehensive understanding of the photophysics in these emerging materials.

INTRODUCTION

Semiconductor nanocrystals (NCs) have many optical and electronic properties that are unique from, and often superior to, their bulk counterparts. These include discrete, size-tunable optical transitions, narrow photoluminescence (PL) linewidths, high photoluminescence quantum yields (PLQYs), and facile solution-based syntheses. This has motivated both fundamental research into these materials as well as the development of NC-based devices and applications. Numerous compositions can be routinely synthesized and have been extensively researched, typically for the II-VI, III-V, and IV-VI families of semiconductors. Recently, ionic perovskite semiconductors have emerged as promising materials for incorporation into optoelectronic devices such as solar cells,[1–3] light-emitting diodes (LEDs),[4,5] and lasers,[6–8] and several inorganic and hybrid organic-inorganic perovskite nanostructures have been successfully synthesized.[9,10] Inorganic cesium lead halide, $CsPbX_3$ (X = Cl, Br, I), perovskite NCs exhibit composition-tunable narrow emission lines and high PLQYs even in the weak electronic confinement regime and without a passivating shell.[10] Metal chalcogenide NCs such as CdSe, in comparison, must be engineered with a passivating semiconductor shell, good ligand coverage, and at sizes comparable to or smaller than the Bohr exciton radius to achieve high PLQYs.

In most covalently-bound semiconductors like silicon, the valence and conduction bands originate from bonding-antibonding orbital pairs. The

presence of defects, for example vacancies, interstitials, and substitutions, results in defect energy levels that can be located deep within the bandgap. These trap states open up nonradiative channels by which the semiconductor can decay, decreasing the PLQY, among other effects. Lead halide perovskites, however, have an electronic structure that is inherently defect tolerant due to a lack of bonding-antibonding interaction between the valence and conduction bands.[11–13] While the valence band maximum originates from the strong antibonding interaction between the Pb 6s and X np atomic orbitals, the empty Pb 6p orbitals couple to form the conduction band minimum.[13] A defect tolerance emerges from this orbital interaction in which most intrinsic defects result in shallow trap states and resonances within the bands. In $CsPbBr_3$, intrinsic defects that do induce deep trap levels have high formation energies (>1 eV) and thus minimal concentrations.[13] While these electronic structure explanations help to justify why lead halide perovskites exhibit a pronounced tolerance to defects, many questions still remain regarding how the absence of deep trap states affects carrier dynamics in perovskite NCs.

An important way to probe the effects of trap states on carrier dynamics is through PL measurements of single NCs. This is because the PL of a single NC fluctuates in time, directly as a result of the interactions between charge carriers and trap states. This PL blinking in single NCs has been studied for two decades in many traditional NC materials and most extensively in CdSe.

There is no single mechanism that can fully account for all the observations of PL blinking behavior, but blinking is consistently attributed to the interaction of charge carriers localizing at defect sites in the NC, at the surface, or external to the NC.[14,15] This charge carrier trapping can be beneficial in certain architectures of photodetectors such as photoconductors if only one type of carrier is localized, but it is undesirable for most optoelectronic devices. Charge trapping introduces nonradiative recombination pathways that are detrimental in LEDs, lasers, and imaging and tracking applications, and it decreases charge mobility and transport, which are crucial parameters in solar cells.

To understand how charge carrier trapping leads to PL blinking, photon counts are typically binned to create a time trajectory of PL intensity, which is then separated into bright, 'on' periods and dark, 'off' periods by applying a threshold level to the trajectory. The series of on and off durations are then used to calculate the corresponding probability distributions of the PL trajectory. In semiconductor NCs, the probability $P(\tau_i)$ of an on or off duration occurring follows a power law, $P(\tau_i) \propto \tau_i^{-\alpha_i}$, where α_i is the power law slope and scaling exponent. The off periods typically obey this simple power law on the timescale of most experiments, while the on periods can be fit to an exponentially-truncated power law, $P(\tau_i) \propto \tau_i^{-\alpha_i} e^{-\tau_i/\tau_c}$, where the truncation time, τ_c, is the time at which the power law kinetics cross-over to

exponential kinetics. The power law behavior of the on ↔ off processes reveals distributed kinetics that have no characteristic time scale. The exponential truncation indicates that either the on → off process at long on durations occurs at a single rate, or the distributed rate process saturates at long on durations.

One class of proposed explanations to account for PL blinking kinetics is based on photoinduced charging. Upon charging of the NC, subsequent excitation leads to nonradiative Auger recombination of a trion that proceeds orders of magnitude faster than radiative recombination, until the NC is reneutralized. Many models of this type have been developed, and typically, their main differences lie in the charging pathway that initiates the on → off process.[16–22] The most widely accepted pathway for photoinduced charging is Auger autoionization, in which one exciton in a biexciton or multiexciton state decays nonradiatively via an energy transfer to ionize one of the charge carriers of the second exciton.[16] Another mechanism that has been very successful in predicting observed PL blinking behavior is the diffusion-controlled electron transfer (DCET) model.[23] Here, the PL suppression (off state) is again attributed to Auger recombination of a trion, but the on → off transitions are not due to Auger autoionization, but are instead facilitated by electron transfer between two displaced Marcus parabolas, corresponding to the neutral and charged NC states. Finally, since several experiments have revealed that Auger trion recombination cannot explain all PL blinking

phenomena, such as a lack of correlation between PL intensity and lifetime[24] and the low PLQY of the off state,[25–27] another set of mechanisms have been proposed that do not involve Auger recombination of charged NCs. These rely on trapping rates that fluctuate with time and can involve a fast removal of a hole to a surface trap state[28,29] or direct trapping of hot electrons to a surface state,[24] followed by rapid nonradiative recombination.

The experimental PL blinking observations that contributed to the development of these theoretical frameworks have been based on semiconductor compositions of type III-V, and IV-VI, and II-VI, with the majority being II-VI materials. How charge carrier trapping occurs in perovskite NCs and how it manifests itself in the PL of a single perovskite NC has not been well established. While several experiments have been carried out, the results have varied widely, and a clear picture has not emerged regarding how NCs without deep intrinsic trap states compare with more traditional semiconductor NC compositions.[30–36] In this work, PL trajectories of over 130 single $CsPbBr_3$ NCs are recorded over four excitation intensities (I_{ex}), without significant photobleaching throughout the total acquisition time for each. The probability distributions of the on and off durations are obtained and the intensity dependence of the power law truncation times considered in the context of PL blinking models. The on-state truncation time is found to initially decrease with excitation intensity, non-quadratically, until a saturation is reached when an average of a single exciton is formed per

pulse. These observations indicate that an Auger autoionization mechanism cannot account for the power law truncation on its own, and the results point towards a DCET mechanism for the on → off trapping process.

METHODS

Weakly confined $CsPbBr_3$ NCs with an edge length of 10 ± 1.5 nm (Bohr exciton diameter of 7 nm[10]) were synthesized following a known procedure.[10] Recent Rietveld refinement and pair distribution function analyses of X-ray total scattering data confirm that the room temperature crystal structure of $CsPbX_3$ NCs is orthorhombic with the space group *Pnma*.[37] A dilute solution of the NCs in toluene was mixed with a 3% Poly(methyl methacrylate)(PMMA)/toluene solution in a 1:1 ratio to help with dispersion, then drop-cast onto a UV-grade fused-silica coverslip. The coverslip was mounted in a modified Olympus IX71 inverted confocal microscope, equipped with a 2D piezoelectric scanning stage (PI 517) and z stage (homebuilt). Pulsed excitation at 400 nm was achieved by the second harmonic of the output of a Coherent RegA9000 amplifier (200 fs, 300 kHz) seeded by a Coherent Mira900 oscillator. The excitation light was focused through a ×100, 1.3 NA oil immersion objective (Nikon PlanFluor) onto the coverslip surface. Fluorescence was collected in an epifluorescence scheme, using a dichroic mirror (Semrock, Di405) and several long-pass and band-pass filters, and focused to two avalanche photodiodes (MPD, PDM-50 series)

that are input to a time-correlated single photon counting (TCSPC) module (PicoQuant, PicoHarp 300).

All measurements were conducted at room temperature, in an ambient atmosphere, and within an average excitation intensity (I_{ex}) range of 2.5 – 17.7 W/cm^2. To determine I_{ex}, the average excitation power was measured directly and the focal spot size area $\left(Area=\pi D^2/4\text{, where D=diameter}\right)$ was calculated from the Gaussian full-width-at-half-maximum (FWHM) of representative emission spot size scans. The average number of excitons formed per pulse was calculated according to $\langle N_{ex}\rangle=\ln(2)\times I_{ex}\frac{\sigma_{¿(\lambda=400\text{nm})}}{E_{\lambda=400\text{nm}}\Gamma_{rep}}¿$, where $E_{\lambda=400\text{nm}}$ is the energy of 400 nm excitation and Γ_{rep} is the laser repetition rate. The absorption cross-section, $\sigma_{¿(\lambda=400\text{nm})¿}$, is the cross-section for single photon absorption (1PA) at 400 nm. We assume that only 1PA events occur under the excitation conditions used here. Two-photon absorption (2PA) has been studied at photon energies below the bandgap, but not at photon energies that compete with ground-state 1PA.[38] We assume the cross-section for 2PA at 400 nm is likewise many orders of magnitude smaller than the one-photon cross-section, requiring very large peak intensities to compete with 1PA. A sequential two-photon process such as excited state absorption (ESA) is another possibility, but the ESA cross-section would need to be larger than the ground-state absorption cross-

section for this to occur. A pump-fluence dependence of the early time (A) and late-time (B) TRPL amplitudes confirms that one exciton is produced from one absorbed photon, which justifies our assumption that multiphoton absorption processes are negligible in these experiments.[39]

10-minute TCSPC measurements were collected for over 130 NCs with ~30 ps resolution, providing a PL trajectory, time-resolved photoluminescence (TRPL) decay, and photon antibunching trace simultaneously. The latter is obtained through the use of a Hanbury Brown and Twiss setup consisting of a 50/50 beamsplitter that separates the emission output onto two separate avalanche photodiodes.

RESULTS AND DISCUSSION

The basic optical properties of the $CsPbBr_3$ NCs investigated here are summarized in **Figure 1**. Ensemble absorption and PL spectra of the NCs dispersed in hexanes, normalized to the band-edge absorption and emission peaks, respectively, are shown in **Figure 1a**. The band-edge absorption peak is at 506 nm and the PL peak is at 512 nm, with a narrow FWHM of ~100 meV. The ensemble PLQY was ~50%. A TRPL measurement for a single NC that is representative of the average is shown in **Figure 1b**. At the lowest I_{ex} used, all NCs decayed bi-exponentially with an average τ_1 = 1.8 $\pm$ 0.6 ns (A_1 = 68%) and τ_2 = 6 $\pm$ 1 ns (A_2 = 32%), within the range of previous

reports at room temperature.[39] A lack of change in the decay times or amplitudes with increasing intensity is observed, which suggests that the faster component may be due to a trap-assisted recombination while the slower component is likely band-edge recombination. Single photon emission at room temperature was observed in single NCs, as evidenced by the lack of a coincidence peak at zero time-delay (photon antibunching) in an example second-order intensity correlation function, $g_2(t)$ (**Figure 1c**). The zero time-delay peak, $g_2(0)$, is consistent with background noise at random delays, while delay times at intervals equal to the inverse laser repetition rate are due to photons detected from subsequent excitation cycles. To ensure all NCs investigated were individual particles, NCs with $g_2(0) > 0.5$ were discarded from further analysis.

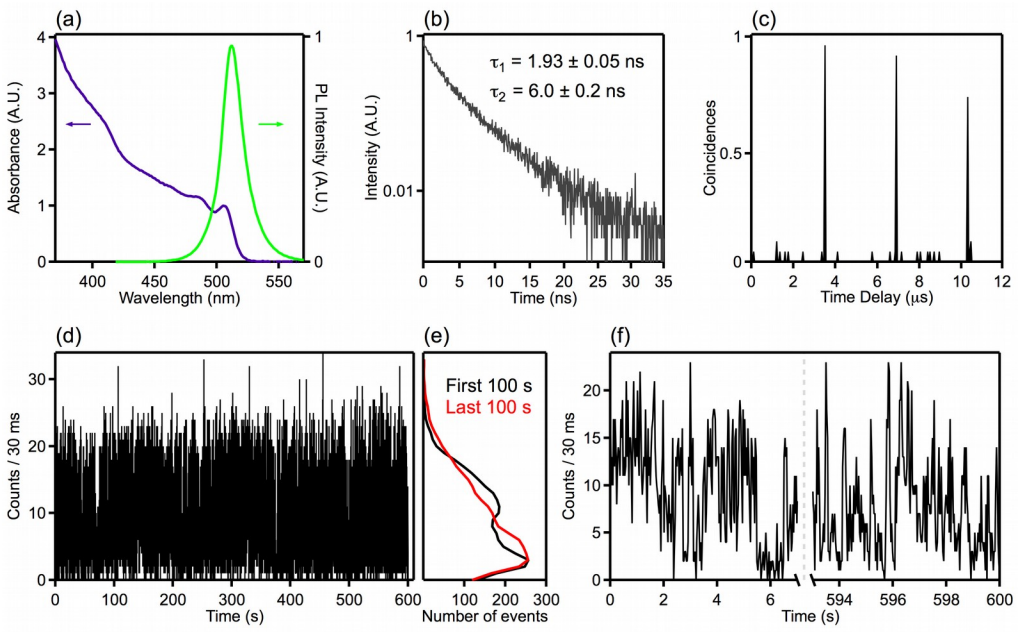

Figure 1. Optical properties of 10 nm $CsPbBr_3$ NCs. All single NC measurements were recorded using an intensity of 2.5 W/cm^2. (a) Absorption

(purple) and PL (green) spectra of $CsPbBr_3$ NCs in hexanes. (b) Representative TRPL and (c) second-order intensity correlation for a single NC. (d) Full 10-minute PL trajectory of a single NC binned at 30 ms with (e) the corresponding PL intensity histogram of the first 100 s (black) and last 100 s (red). (f) Same PL trajectory as in (d) showing only the first and last 7 s time intervals.

The repetition rate of the laser used in these experiments, 300 kHz, is an order of magnitude lower than the 1-10 MHz rates often used in pulsed, single NC experiments. This appears to be essential for acquiring PL trajectories of single NCs for long durations without substantial photobleaching. A representative 10-minute trajectory of a single NC binned at 30 ms, shown in **Figure 1d**, demonstrates the lack of PL bleaching over this time scale. Corresponding histograms of the PL intensity during the first and last 100 s are displayed in **Figure 1e**; notably, the overall PL intensity counts do not significantly change, but lower emission intensities are observed to increase in frequency while the higher emission intensities decrease in frequency between the first and last 100 s of the PL trajectory. A subset of the trajectory is shown in **Figure 1f**, which further illustrates the consistency in PL behavior throughout the acquisition time. In comparison, previous work using a 2 MHz excitation source reported significant bleaching in $CsPbBr_3$ NCs after less than one minute of excitation.[33]

The results in **Figure 1** are characteristic for NCs measured at the lowest I_{ex}. At higher I_{ex}, a small decrease in PL counts does accompany the frequency change between the first and last 100 s, and a larger portion of the NCs are completely photobleached in less than 10 minutes. The I_{ex} values used and the number of NCs analyzed at each intensity are summarized in **Table 1**, as well as the percentage of NCs that completely photobleached within the acquisition time. This includes a fairly small percentage of NCs at the lowest three intensities, but 17 of the 24 NCs excited at the highest intensity of 17.7 W/cm^2 experienced photobleaching within 10 minutes.

Table 1. Excitation intensities and photobleaching statistics of NCs measured.

I_{ex} (W/cm^2)	**Number of NCs**	**NC photobleached < 10 min (%)**
2.5	39	0
4.4	35	17
8.8	36	17
17.7	24	71

While the low repetition rate largely enables long acquisition times with minimal photobleaching, a drawback is a reduction in the overall PL counts per second. When the photon counts from the PL trajectories are binned at 30 ms, the peaks in the PL intensity histograms overlap significantly (see

Figure 1e and **Figure S1**). This prevents the histograms from being reliably resolved into a distinguishable number of Gaussian peaks. As a result, the choice of a threshold value to separate the PL trajectories into on and off states becomes somewhat arbitrary and can greatly affect the resulting probability distributions.[40,41] The choice of bin time has also been found to affect the power law parameters, particularly the on-state truncation time.[40,41] To avoid binning and thresholding biases, changepoint analysis (CPA) was used instead to determine the number of intensity levels in each PL trajectory. The CPA algorithm uses a generalized likelihood ratio test to identify locations in the raw photon arrival times where intensity change points occur.[42] The Bayesian information criterion is used to cluster change points into a discrete number of intensity levels. With the number and location of intensity changes determined, a bin-free PL trajectory can be reconstructed. An example comparing the two analysis methods is shown in **Figure 2** for a NC excited at 2.5 W/cm^2. **Figure S1** provides additional examples of representative PL intensity histograms at each I_{ex}.

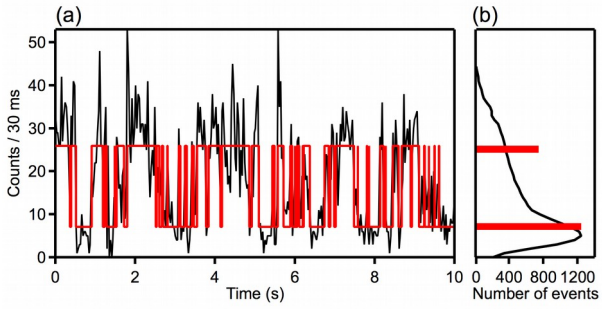

Figure 2. PL trajectories and histograms obtained using two different analysis methods for a NC excited at 2.5 W/cm^2. (a) 10 s of a PL trajectory

binned at 30 ms in black, overlaid with corresponding CPA trajectory in red. (b) Intensity histograms for both methods.

Probability distributions were obtained using the CPA trajectories. The lowest intensity level is considered the off state, while the higher levels are considered on states. At the four I_{ex} used here, the average number of intensity levels detected using the CPA algorithm did not change ($\langle N_{levels} \rangle$=¿ 2.7 levels for 2.5, 8.8, and 17.7 W/cm^2; $\langle N_{levels} \rangle$=¿ 2.6 levels for 4.4 W/cm^2). As such, the probability distributions for all on-state levels were grouped together for improved statistics. On-state probability distributions from individual NCs that are representative across the range of excitation intensities are shown in **Figure 3a**. The probability distributions follow exponentially-truncated power laws that truncate at earlier times with increasing excitation intensity. The truncation times, τ_c, for all NC probability distributions that could be reliably fit to a truncated power law are summarized in **Figure 3b**. The distribution of τ_c shifts towards smaller values with increasing I_{ex}.

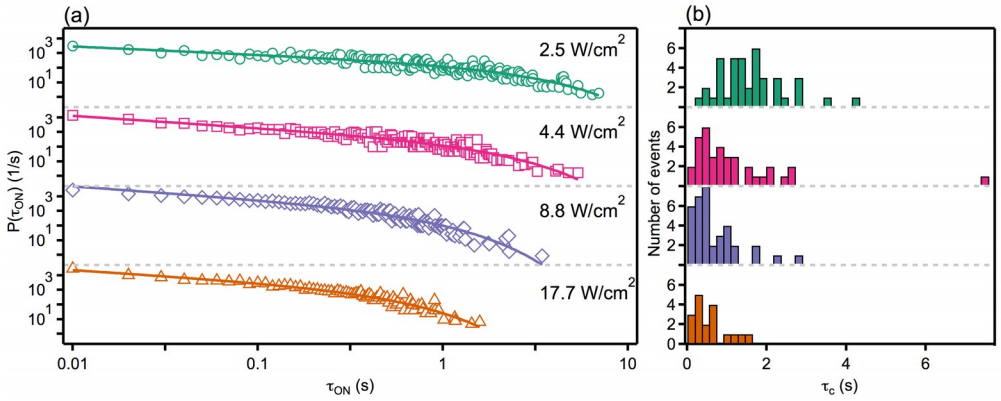

Figure 3. (a) Sample on-state probability distributions at each I_{ex} that follow truncated power laws. (b) Corresponding distribution of on-state truncation times for all NCs that could be fit to a truncated power law.

At all intensities used, the average power law slope (α_{on}) is <1.2, indicating that on-state probability distributions of $CsPbBr_3$ NCs are observed to decay more slowly compared to chalcogenide NCs such as CdSe, where α_{on} is consistently between 1.2-1.8.[19,21,43,44] On-state truncation times vary more considerably in the literature due to their demonstrated sensitivity to various experimental conditions such as photon excitation energy, excitation intensity, dielectric constant of the surrounding media, and shell thickness. An experiment in which the photon excitation energy was identical to that used here, 650 meV above the bandgap, and the sample preparation consistent (dilute solution of NCs mixed with PMMA/toluene), the average truncation time for CdSe/ZnS NCs was <0.1 s at an average exciton formation of $\langle N_{ex} \rangle$=0.28.[43] In comparison, at $\langle N_{ex} \rangle$=0.3 in this experiment, the average truncation time was 1.61 s. Broadly, a reduction in α_{on} and an increase in τ_c suggest that $CsPbBr_3$ NCs tend towards longer on durations than traditional NC materials such as CdSe.

The cause of the truncation of power law kinetics can be investigated by examining the intensity dependence of the truncation time in more detail. The average inverse truncation time, $1/\tau_c$, is displayed as a function of excitation intensity in **Figure 4a**. The *x* axis error bars include the error

associated with measuring the average power and excitation spot size, while the grey shading in the *y* axis direction corresponds to the standard deviation in $1/\tau_c$. The data spread in $1/\tau_c$ can be partially attributed to the large sample size dispersity as the absorption cross-section of $CsPbBr_3$ NCs has been shown to vary linearly with the NC volume at 3.1 eV.[39] This is typical for NCs excited at energies far above the band-edge as the NC absorption spectrum converges into the bulk spectrum. Since the average number of excitons formed per pulse is proportional to the size-dependent cross-section, $\langle N_{ex} \rangle = \ln(2) \times I_{ex} \frac{\sigma_{¡ú(\lambda=400\,\mathrm{nm})}}{E_{\lambda=400\,\mathrm{nm}} \Gamma_{rep}}$¿, changes in the NC volume directly propagate through to $\langle N_{ex} \rangle$. Therefore, the sample size dispersity is expected to be partially responsible for the large data spread at each intensity point in **Figure 4a** given that $1/\tau_c$ is dependent on $\langle N_{ex} \rangle$, which in turn is affected by the NC volume. Differences in the local dielectric environment surrounding each NC may be a contributor as well, namely the configuration of oleylammonium ligands and PMMA matrix surrounding each individual NC.

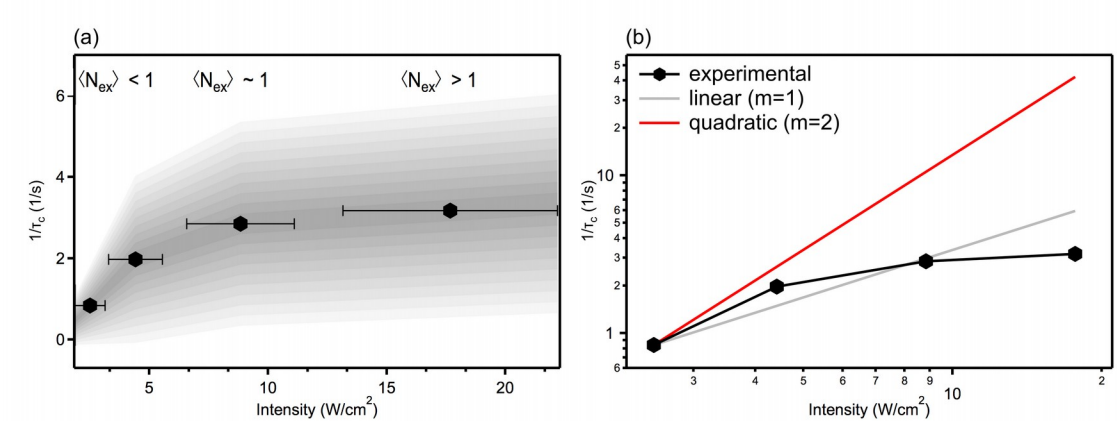

Figure 4. (a) Average inverse truncation time, $1/\tau_c$, at each I_{ex} used, with the error given by the grey shading. The regimes of excitation in terms of exciton formation are labelled. (b) Expected $1/\tau_c$ results for a quadratic (red) and linear (grey) intensity dependence, shown with the experimentally measured values (black), on a logarithmic-logarithmic scale.

The average absorption cross-section for 10 nm $CsPbBr_3$ NCs was calculated using the volume scaling reported by Makarov et al.[39] A value of $\sigma_{|\dot{\iota}|(\lambda=400\,\mathrm{nm},\ 10\ \mathrm{nm\ NC})}=1.6\pm0.7\times10^{-14}\ \mathrm{cm}^2$ is extracted, where the error takes into account the sample size dispersity of 15%. This is comparable to our estimate obtained via scattering-corrected absorbance measurements of $\sigma_{|\dot{\iota}|(\lambda=400\,\mathrm{nm},\ 10\ \mathrm{nm\ NC})}=2.1\pm0.2\times10^{-14}\ \mathrm{cm}^2$. More details regarding this estimation are provided in the Supplementary Information and in **Figure S2**. Using the former cross-section value, which we deem more reliable, the average numbers of excitons created per pulse at the four intensities used in this experiment are $\langle N_{ex}\rangle \sim 0.3$, 0.5, 1, and 2, and the features in **Figure 4a** can

then be grouped into two regions: an increase in $1/\tau_c$ with increasing intensity at $\langle N_{ex} \rangle < 1$, and a saturation near $\langle N_{ex} \rangle \approx 1$.

At the lowest intensities, extracting a precise value of m, to determine the functional form $\frac{1}{\tau_c} \propto I_{ex}{}^{m}$, cannot be done with significance given there are only two data points, although it does appear to be lower than m = 2. A quadratic dependence with m = 2, which has been observed experimentally in chalcogenide compositions, would suggest that the exponential truncation of power law kinetics is due to Auger autoionization of a biexciton, where the rate of biexciton formation scales quadratically with excitation intensity.[43,45] Conversely, the DCET model predicts a linear intensity dependence of the truncation time with m = 1,[23,28] which has also been observed experimentally.[21,46] Within the framework of the DCET model, a random walk along diffusing energy surfaces results in on ↔ off transitions when the neutral and charged energy surfaces intersect. The parabolic shape of the energy surfaces naturally results in a saturation of the power law dynamics and leads to an exponential truncation, which is predicted to be inversely proportional to the diffusion time and thus to the intensity. The multiple recombination centers (MRC) model is a proposed mechanism that has successfully described the observed PL dynamics in NCs as well as nanorods, nanowires, and organic molecules in a glassy environment.[29,47] In the MRC model framework, a distribution of surface trap sites that randomly switch

between active and inactive states gives rise to fluctuating trapping rates. While an intensity dependence is expected to exist, since the change in the trap conformation is assumed to be light-induced, the mechanism of this switching process has not been determined; therefore, the expected value of m for the MRC model is unknown.

The expected results for both a linear and quadratic intensity dependence are shown in **Figure 4b,** along with the experimentally measured $1/\tau_c$ data. In the excitation regime of $\langle N_{ex} \rangle < 1$, it appears that $1<m<2$, which agrees with results reported at low intensities for $CsPbI_3$ NCs ($m=1.3$).[33] This suggests that a combination of PL blinking mechanisms are responsible for the intensity dependent results presented here. The role of multi-excitons cannot be ignored given the non-negligible probability of their formation (for example, 3% biexcitons per pulse at the lowest intensity used); however, if Auger autoionization was solely responsible for the power law truncation, a quadratic dependence with $m=2$ should be observed. As the repetition rate used here allows NCs to be excited at even higher intensities without rapid photobleaching, we are able to observe a saturation in $1/\tau_c$ near $\langle N_{ex} \rangle \approx 1$. This behavior also contradicts what would be expected if the dominant mechanism were Auger autoionization, where such a substantial saturation should not occur until $\langle N_{ex} \rangle \approx 2$. Cordones et al. observed that CdSe/ZnS NCs exhibited a saturation in the off-state probability distributions at $\langle N_{ex} \rangle \approx 1$ and

a saturation in the on-state truncation time at $\langle N_{ex} \rangle \approx 2$.[14] The DCET mechanism was invoked to explain the off-state saturation at a single exciton, while an Auger ionization mechanism was proposed to account for the on-state saturation at a biexciton.

In contrast, a DCET mechanism appears to be the likely trapping mechanism responsible for the on → off kinetics observed in $CsPbBr_3$ NCs. A small contribution from an Auger mechanism would account for the observed results at low intensities where 1<m<2, but the dominant mechanism must be diffusion-based to account for the saturation behavior at $\langle N_{ex} \rangle \approx 1$. In **Figure S3**, the truncation time is plotted against the probability of forming two or more excitons as further evidence that Auger autoionization is not primarily responsible for the on-state truncation (more details in the Supplementary Information). Several other reports have examined PL blinking in $CsPbX_3$ NCs of size similar to the NCs presented here, including at different excitation intensities, but the presented results have varied considerably.[30–33,48] Flickering of the PL has been reported, where the PL blinks between a bright state and a dim but not off state with short dim-time bursts of <60 ms,[31] while binary on-off blinking has also been reported.[33] Photoactivation at higher powers has been observed and attributed to light-induced structural reorganization,[32] as well as rapid PL bleaching even at low excitation intensities.[33]

The lack of a cohesive picture of PL blinking and in general the charge dynamics in perovskite nanocrystals highlights the need for further experimental and theoretical study. An analogous experiment to the one presented here could be carried out with lower photon excitation energies. Not only would this reduce the size dependence of the absorption cross-section, but the experiments would create charge carriers that are less hot. In the present experiment, the excess photon energy is 650 meV, so PL blinking dynamics obtained with an excitation energy closer to the band-edge could provide insight into the role of hot carriers in perovskite NCs. The evolving synthetic field can also extend the experimental capabilities. For example, the addition of a passivating shell would provide a barrier to charge ejection, likely extending the on durations and tuning the PL blinking behavior. New ligands that provide more passivating coverage of the NC surface will also affect the carrier dynamics. In addition, achieving higher monodispersity should produce trends with greater certainty, while new stabilization and dispersion techniques will allow for a comparison between polymer and polymer-free external environments.

CONCLUSIONS

In contrast to chalcogenide NCs, perovskite $CsPbBr_3$ NCs in only the weak confinement regime and without a passivating shell display bright PL that can largely be attributed to the material’s inherent defect tolerance. In this

work, PL trajectories were recorded for over 130 $CsPbBr_3$ perovskite NCs using a range of excitation intensities $\left(\langle N_{ex}\rangle = 0.3-2\right)$. Minimal photobleaching due to the low repetition rate laser combined with the use of the changepoint analysis method were important to achieve a reliable extraction of kinetics. The on-state probability distributions at all intensities yielded an average $\alpha_{on} < 1$ and $\tau_c > 0.5$ s, revealing that perovskite NCs tend towards longer on durations than traditional chalcogenide NC compositions. In the excitation regime of $\langle N_{ex}\rangle < 1$, the on-state truncation time decreases with increasing excitation intensity according to $\frac{1}{\tau_c} \propto {I_{ex}}^m$, where 1<m<2. A saturation is observed near $\langle N_{ex}\rangle \approx 1$, indicating that the on $\rightarrow$ off trapping process is most likely dominated by a DCET blinking mechanism, with a smaller contribution from Auger autoionization. Continued experiments and theoretical studies are required to investigate the mechanism of PL blinking in defect tolerant semiconductor NCs such as the lead halide perovskites, and more broadly, to understand how these materials compare to traditional semiconductors.

ASSOCIATED CONTENT

Supporting Information. Sample PL intensity histograms at all intensities, estimation of absorption cross-section, and truncation time as a function of multi-exciton formation probability.

AUTHOR INFORMATION

Corresponding Author

*E-mail: srl@berkeley.edu. Telephone: +1 510-643-5467.

Author Contributions

The manuscript was written through contributions of all authors. All authors have given approval to the final version of the manuscript.

Notes

The authors declare no competing financial interest.

ACKNOWLEDGMENT

This work was funded by the U.S. Department of Energy, Office of Science, Office of Basic Energy Sciences, Materials Sciences and Engineering Division under Contract No. DE-AC02-05-CH11231 (Physical Chemistry of Inorganic Nanostructures Program KC3103).

REFERENCES

(1) Green, M. A.; Ho-Baillie, A.; Snaith, H. J. The Emergence of Perovskite

Solar Cells. *Nat. Photonics* **2014**, *8*, 506–514.

(2) Zhou, H.; Chen, Q.; Li, G.; Luo, S.; Song, T. B.; Duan, H. S.; Hong, Z.; You, J.; Liu, Y.; Yang, Y. Interface Engineering of Highly Efficient Perovskite Solar Cells. *Science* **2014**, *345*, 542–546.

(3) Jeon, N. J.; Noh, J. H.; Yang, W. S.; Kim, Y. C.; Ryu, S.; Seo, J.; Seok, S. II. Compositional Engineering of Perovskite Materials for High-Performance Solar Cells. *Nature* **2015**, *517*, 476–480.

(4) Tan, Z. K.; Moghaddam, R. S.; Lai, M. L.; Docampo, P.; Higler, R.; Deschler, F.; Price, M.; Sadhanala, A.; Pazos, L. M.; Credgington, D.; et al. Bright Light-Emitting Diodes Based on Organometal Halide Perovskite. *Nat. Nanotechnol.* **2014**, *9*, 687–692.

(5) Li, G.; Tan, Z. K.; Di, D.; Lai, M. L.; Jiang, L.; Lim, J. H. W.; Friend, R. H.; Greenham, N. C. Efficient Light-Emitting Diodes Based on Nanocrystalline Perovskite in a Dielectric Polymer Matrix. *Nano Lett.* **2015**, *15*, 2640–2644.

(6) Xing, G.; Mathews, N.; Lim, S. S.; Yantara, N.; Liu, X.; Sabba, D.; Grätzel, M.; Mhaisalkar, S.; Sum, T. C. Low-Temperature Solution-Processed Wavelength-Tunable Perovskites for Lasing. *Nat. Mater.* **2014**, *13*, 476–480.

(7) Eaton, S. W.; Lai, M.; Gibson, N. A.; Wong, A. B.; Dou, L.; Ma, J.; Wang, L.-W.; Leone, S. R.; Yang, P. Lasing in Robust Cesium Lead Halide Perovskite Nanowires. *Proc. Natl. Acad. Sci. U. S. A.* **2016**, *113*, 1993–1998.

(8) Zhu, H.; Fu, Y.; Meng, F.; Wu, X.; Gong, Z.; Ding, Q.; Gustafsson, M. V; Trinh, M. T.; Jin, S.; Zhu, X.-Y. Lead Halide Perovskite Nanowire Lasers with Low Lasing Thresholds and High Quality Factors. *Nat. Mater.* **2015**, *14*, 636–642.

(9) Bekenstein, Y.; Koscher, B. A.; Eaton, S. W.; Yang, P.; Alivisatos, A. P. Highly Luminescent Colloidal Nanoplates of Perovskite Cesium Lead Halide and Their Oriented Assemblies. *J. Am. Chem. Soc.* **2015**, *137*, 16008–16011.

(10) Protesescu, L.; Yakunin, S.; Bodnarchuk, M. I.; Krieg, F.; Caputo, R.; Hendon, C. H.; Yang, R. X.; Walsh, A.; Kovalenko, M. V. Nanocrystals of Cesium Lead Halide Perovskites ($CsPbX_3$, X = Cl, Br, and I): Novel Optoelectronic Materials Showing Bright Emission with Wide Color Gamut. *Nano Lett.* **2015**, *15*, 3692–3696.

(11) Buin, A.; Pietsch, P.; Xu, J.; Voznyy, O.; Ip, A. H.; Comin, R.; Sargent, E. H. Materials Processing Routes to Trap-Free Halide Perovskites. *Nano Lett.* **2014**, *14*, 6281–6286.

(12) Brandt, R. E.; Stevanović, V.; Ginley, D. S.; Buonassisi, T. Identifying Defect-Tolerant Semiconductors with High Minority-Carrier Lifetimes: Beyond Hybrid Lead Halide Perovskites. *MRS Commun.* **2015**, *5*, 265–275.

(13) Kang, J.; Wang, L.-W. High Defect Tolerance in Lead Halide Perovskite $CsPbBr_3$. *J. Phys. Chem. Lett.* **2017**, *8*, 489–493.

(14) Cordones, A. A.; Leone, S. R. Mechanisms for Charge Trapping in Single

Semiconductor Nanocrystals Probed by Fluorescence Blinking. *Chem. Soc. Rev.* **2013**, *42*, 3209–3221.

(15) Schwartz, O.; Oron, D. A Present Understanding of Colloidal Quantum Dot Blinking. *Isr. J. Chem.* **2012**, *52*, 992–1001.

(16) Nirmal, M.; Dabbousi, B.; Bawendi, M.; Macklin, J.; Trautman, J.; Harris, T.; Brus, L. Fluorescence Intermittency in Single Cadmium Selenide Nanocrystals. *Nature* **1996**, *383*, 802–804.

(17) Efros, A. F.; Rosen, M. Random Telegraph Signal in the Photoluminescence Intensity of a Single Quantum Dot. *Phys. Rev. Lett.* **1997**, *78*, 1110–1113.

(18) Verberk, R.; van Oijen, A.; Orrit, M. Simple Model for the Power-Law Blinking of Single Semiconductor Nanocrystals. *Phys. Rev. B* **2002**, *66*, 233202/1-233202/4.

(19) Kuno, M.; Fromm, D. P.; Hamann, H. F.; Gallagher, A.; Nesbitt, D. J. “On”/“off” Fluorescence Intermittency of Single Semiconductor Quantum Dots. *J. Chem. Phys.* **2001**, *115*, 1028–1040.

(20) Tang, J.; Marcus, R. A. Diffusion-Controlled Electron Transfer Processes and Power-Law Statistics of Fluorescence Intermittency of Nanoparticles. *Phys. Rev. Lett.* **2005**, *95*, 107401/1-107401/4.

(21) Shimizu, K. T.; Neuhauser, R. G.; Leatherdale, C. A.; Empedocles, S. A.; Woo, W. K.; Bawendi, M. G. Blinking Statistics in Single Semiconductor Nanocrystal Quantum Dots. *Phys. Rev. B* **2001**, *63*, 205316/1-205316/5.

(22) Osborne, M. A.; Fisher, A. A. E. Charge-Tunnelling and Self-Trapping:

Common Origins for Blinking, Grey-State Emission and Photoluminescence Enhancement in Semiconductor Quantum Dots. *Nanoscale* **2016**, *8*, 9272–9283.

(23) Tang, J.; Marcus, R. A. Mechanisms of Fluorescence Blinking in Semiconductor Nanocrystal Quantum Dots. *J. Chem. Phys.* **2005**, *123*, 054704/1-054704/12.

(24) Galland, C.; Ghosh, Y.; Steinbrück, A.; Sykora, M.; Hollingsworth, J. A.; Klimov, V. I.; Htoon, H. Two Types of Luminescence Blinking Revealed by Spectroelectrochemistry of Single Quantum Dots. *Nature* **2011**, *479*, 203–207.

(25) Califano, M. Off-State Quantum Yields in the Presence of Surface Trap States in CdSe Nanocrystals: The Inadequacy of the Charging Model to Explain Blinking. *J. Phys. Chem. C* **2011**, *115*, 18051–18054.

(26) Jha, P. P.; Guyot-Sionnest, P. Trion Decay in Colloidal Quantum Dots. *ACS Nano* **2009**, *3*, 1011–1015.

(27) Zhao, J.; Nair, G.; Fisher, B. R.; Bawendi, M. G. Challenge to the Charging Model of Semiconductor-Nanocrystal Fluorescence Intermittency from Off-State Quantum Yields and Multiexciton Blinking. *Phys. Rev. Lett.* **2010**, *104*, 157403/1-157403/4.

(28) Frantsuzov, P. A.; Marcus, R. A. Explanation of Quantum Dot Blinking without the Long-Lived Trap Hypothesis. *Phys. Rev. B* **2005**, *72*, 155321/1-155321/10.

(29) Frantsuzov, P. A.; Volkán-Kacsó, S.; Jankó, B. Model of Fluorescence

Intermittency of Single Colloidal Semiconductor Quantum Dots Using Multiple Recombination Centers. *Phys. Rev. Lett.* **2009**, *103*, 207402/1-207402/4.

(30) Hu, F.; Zhang, H.; Sun, C.; Yin, C.; Lv, B.; Zhang, C.; Yu, W. W.; Wang, X.; Zhang, Y.; Xiao, M. Superior Optical Properties of Perovskite Nanocrystals as Single Photon Emitters. *ACS Nano* **2015**, *9*, 12410–12416.

(31) Swarnkar, A.; Chulliyil, R.; Ravi, V. K.; Irfanullah, M.; Chowdhury, A.; Nag, A. Colloidal $CsPbBr_3$ Perovskite Nanocrystals: Luminescence beyond Traditional Quantum Dots. *Angew. Chemie - Int. Ed.* **2015**, *54*, 15424–15428.

(32) Seth, S.; Mondal, N.; Patra, S.; Samanta, A. Fluorescence Blinking and Photoactivation of All-Inorganic Perovskite Nanocrystals $CsPbBr_3$ and $CsPbBr_2I$. *J. Phys. Chem. Lett.* **2016**, *7*, 266–271.

(33) Park, Y.-S.; Guo, S.; Makarov, N.; Klimov, V. I. Room Temperature Single-Photon Emission from Individual Perovskite Quantum Dots. *ACS Nano* **2015**, *9*, 10386–10393.

(34) Wen, X.; Ho-Baillie, A.; Huang, S.; Sheng, R.; Chen, S.; Ko, H. C.; Green, M. A. Mobile Charge-Induced Fluorescence Intermittency in Methylammonium Lead Bromide Perovskite. *Nano Lett.* **2015**, *15*, 4644–4649.

(35) Tian, Y.; Merdasa, A.; Peter, M.; Abdellah, M.; Zheng, K.; Ponseca, C. S.; Pullerits, T.; Yartsev, A.; Sundström, V.; Scheblykin, I. G. Giant

Photoluminescence Blinking of Perovskite Nanocrystals Reveals Single-Trap Control of Luminescence. *Nano Lett.* **2015**, *15*, 1603–1608.

(36) Tachikawa, T.; Karimata, I.; Kobori, Y. Surface Charge Trapping in Organolead Halide Perovskites Explored by Single-Particle Photoluminescence Imaging. *J. Phys. Chem. Lett.* **2015**, *6*, 3195–3201.

(37) Cottingham, P.; Brutchey, R. L. On the Crystal Structure of Colloidally Prepared CsPbBr $_3$ Quantum Dots. *Chem. Commun.* **2016**, *52*, 5246–5249.

(38) Chen, J.; Žídek, K.; Chábera, P.; Liu, D.; Cheng, P.; Nuuttila, L.; Al-Marri, M. J.; Lehtivuori, H.; Messing, M. E.; Han, K.; et al. Size- and Wavelength-Dependent Two-Photon Absorption Cross-Section of $CsPbBr_3$ Perovskite Quantum Dots. *J. Phys. Chem. Lett.* **2017**, *8*, 2316–2321.

(39) Makarov, N. S.; Guo, S.; Isaienko, O.; Liu, W.; Robel, I.; Klimov, V. I. Spectral and Dynamical Properties of Single Excitons, Biexcitons, and Trions in Cesium-Lead-Halide Perovskite Quantum Dots. *Nano Lett.* **2016**, *16*, 2349–2362.

(40) Crouch, C. H.; Sauter, O.; Wu, X.; Purcell, R.; Querner, C.; Drndic, M.; Pelton, M. Facts and Artifacts in the Blinking Statistics of Semiconductor Nanocrystals. *Nano Lett.* **2010**, *10*, 1692–1698.

(41) Bae, Y. J.; Gibson, N. A.; Ding, T. X.; Alivisatos, A. P.; Leone, S. R. Understanding the Bias Introduced in Quantum Dot Blinking Using Change Point Analysis. *J. Phys. Chem. C* **2016**, *120*, 29484–29490.

(42) Watkins, L. P.; Yang, H. Detection of Intensity Change Points in Time-Resolved Single-Molecule Measurements. *J. Phys. Chem. B* **2005**, *109*, 617–628.

(43) Peterson, J. J.; Nesbitt, D. J. Modified Power Law Behavior in Quantum Dot Blinking: A Novel Role for Biexcitons and Auger Ionization. *Nano Lett.* **2009**, *9*, 338–345.

(44) Houel, J.; Doan, Q. T.; Cajgfinger, T.; Ledoux, G.; Amans, D.; Aubret, A.; Dominjon, A.; Ferriol, S.; Barbier, R.; Nasilowski, M.; et al. Autocorrelation Analysis for the Unbiased Determination of Power-Law Exponents in Single-Quantum-Dot Blinking. *ACS Nano* **2015**, *9*, 886–893.

(45) Early, K. T.; Nesbitt, D. J. Size-Dependent Photoionization in Single CdSe/ZnS Nanocrystals. *Nano Lett.* **2013**, *13*, 4844–4849.

(46) Stefani, F. D.; Knoll, W.; Kreiter, M.; Zhong, X.; Han, M. Y. Quantification of Photoinduced and Spontaneous Quantum-Dot Luminescence Blinking. *Phys. Rev. B* **2005**, *72*, 125304/1-125304/7.

(47) Frantsuzov, P. A.; Volkán-Kacsó, S.; Jankó, B. Universality of the Fluorescence Intermittency in Nanoscale Systems: Experiment and Theory. *Nano Lett.* **2013**, *13*, 402–408.

(48) Rainoì, G.; Nedelcu, G.; Protesescu, L.; Bodnarchuk, M. I.; Kovalenko, M. V.; Mahrt, R. F.; Stöferle, T. Single Cesium Lead Halide Perovskite Nanocrystals at Low Temperature: Fast Single-Photon Emission, Reduced Blinking, and Exciton Fine Structure. *ACS Nano* **2016**, *10*,

2485–2490.

SYNOPSIS

For Table of Contents Only: